Upwards Tropospheric Influence on Tropical Stratospheric Upwelling

Under peer review

Jonathan Lin[a,c] Kerry Emanuel, [b]

[a] *Lamont-Doherty Earth Observatory, Columbia University, New York, New York*
[b] *Lorenz Center, Department of Earth, Atmospheric, and Planetary Sciences, Massachusetts Institute of Technology, Cambridge, Massachusetts*
[c] *Department of Earth and Atmospheric Sciences, Cornell University, Ithaca, New York*

ABSTRACT: The response of the stratosphere to a steady geopotential forcing is considered in two separate theoretical models. Solutions to the linearized quasi-geostrophic potential vorticity equations are first used to show that the vertical length scale of a tropopause geopotential anomaly is initially shallow, but significantly increased by diabatic heating from radiative relaxation. This process is deemed as geostrophic adjustment of the stratosphere to tropospheric forcing. Idealized, time-dependent calculations show that tropopause geopotential anomalies can appreciably rise in the stratosphere on time scales of a couple months. A previously developed, coupled troposphere-stratosphere model is introduced and modified to further understand how tropospheric geopotential forcing can induce upwelling in the stratosphere. Solutions to steady, zonally-symmetric sea-surface-temperature forcings in the linear β-plane model show that the upwards stratospheric penetration of the thermally induced tropopause geopotential anomaly is controlled by a non-dimensional parameter that depends on the ratio between the time scale of wave-drag to that of radiation. It is also shown that the horizontal scale of the tropopause geopotential anomaly modulates the vertical scale of the anomaly. When Earth-like non-dimensional parameters are used, the theoretical model predicts stratospheric temperature anomalies around two times larger in magnitude than those in the boundary layer, approximately in line with observational data. The results are argued to show that wave-drag alone may not suffice to explain certain observed features of the lower stratosphere, foremost of which is the anti-correlation between sea-surface temperature and lower stratospheric temperature.

SIGNIFICANCE STATEMENT: Upwards motion in the tropical stratosphere, the layer of atmosphere above where most weather occurs, is thought to be controlled by weather disturbances that propagate upwards and dissipate in the stratosphere. The strength of this upwards motion is important since it sets the global distribution of ozone. We formulate and use simple mathematical models to show the vertical motion in the stratosphere can also depend on the warming in the troposphere, the layer of atmosphere where humans live. We use the theory as an explanation for our observations of inverse correlations between the ocean temperature and the stratosphere temperature. These findings imply that cooling in the stratosphere may be tightly coupled to ocean warming.

1. Introduction

The Brewer-Dobson circulation (BDC) is a global-scale overturning circulation in the stratosphere, characterized by air that ascends into and within the tropical stratosphere, spreading poleward and eventually downwards in the extratropical winter-hemisphere. This stratospheric circulation can significantly impact tropospheric climate, most notably through its modulation of the distribution of stratospheric ozone, which absorbs harmful UV radiation from the sun (Dobson 1956). The widely accepted mechanism that explains the existence of the BDC is the principle of "downward control" (Haynes and McIntyre 1987; Haynes et al. 1991). This principle states that the upward mass flux across a specified vertical level is solely a function of the zonal momentum sources and sinks above that level; thus, processes in the middle and upper stratosphere can exert a "downward" influence on flow in the lower stratosphere and troposphere. In the stratosphere and mesosphere, it is primarily the dissipation of upward propagating Rossby and gravity waves that contributes zonal momentum (Seviour et al. 2012). The theoretical findings of Haynes and McIntyre (1987) have been well supported by numerical modeling evidence and withstood the test of time (Butchart 2014, and references therein). Thus, in the "downward control" paradigm, wave dissipation drives the circulation.

The BDC is typically separated into two branches: a slow and deep equator-to-pole overturning branch, and a faster shallow branch in the lower stratosphere extending to about 50° latitude (Plumb 2002; Birner and Bönisch 2011). The deep branch is thought to be driven by planetary scale waves breaking in the middle and upper portions of the stratosphere, a process also known as the extratropical pump (Holton et al. 1995). The shallow branch is thought to be driven by sub-tropical wave-dissipation in the lower stratosphere (Plumb and Eluszkiewicz 1999; Plumb 2002). In this study, we focus primarily on the shallow branch circulation, and, in particular, its connections to the troposphere.

Corresponding author: Jonathan Lin, jlin@ldeo.columbia.edu

In the tropical stratosphere, upwelling strength is strongly correlated with tropical stratospheric temperature, as on slow time scales, a cold anomaly in the stratosphere is radiatively heated, which is balanced by adiabatic cooling (Randel et al. 2006; Kerr-Munslow and Norton 2006). Thus, understanding the processes that control the strength of upwelling in the lower stratosphere and the tropical tropopause layer (TTL) is crucial to determining the temperature of these layers (Fueglistaler et al. 2009). The temperature in the TTL region is crucial since it has been linked with the concentration of both water vapor and ozone in the stratosphere (Jensen and Pfister 2004; Randel et al. 2006).

In our opinion, there are a few characteristics of the shallow branch circulation that remained unresolved. First, calculations of residual vertical velocities at 70-hPa indicate off-equator maxima in shallow branch upwelling in the summer-time hemisphere (Randel et al. 2008; Seviour et al. 2012). Wave-drag is at its annual maximum in the winter hemisphere, which is thus at odds with the observation of tropical upwelling maximizing in the summer-time hemisphere, though wave-drag can force circulations non-linearly and non-locally (Holton et al. 1995; Plumb and Eluszkiewicz 1999). Plumb and Eluszkiewicz (1999, hereafter, PE99) also elegantly pointed out that mid-latitude wave driving of the Brewer-Dobson circulation cannot explain observations of mean upwelling in the tropical stratosphere, and showed that either thermal forcing or sub-tropical wave drag is necessary to produce tropical upwelling over the equator. Indeed, many studies have focused on not just the role extratropical wave-dissipation plays in modulating the upwelling strength of the TTL and lower stratosphere (Taguchi 2009; Garny et al. 2011; Kim et al. 2016), but also that of tropical/sub-tropical wave-drag (Boehm and Lee 2003; Norton 2006; Randel et al. 2008; Ryu and Lee 2010; Ortland and Alexander 2014; Jucker and Gerber 2017).

Naturally, many of these studies invoke the downward control paradigm. However, PE99 found that the existence of a thermally-forced circulation in the stratosphere and the breakdown of downward control theory go together. This led PE99 to question the generality of downward control in the deep tropics, and whether or not thermally forced tropospheric circulations could “leak" upwards into the stratosphere (for the time being, we remain imprecise on the meaning of “leak"). As suggested by PE99, stratospheric “leakage" of the Hadley cell does not have to be very large to make a substantial difference to the stratospheric circulation, since mid-tropospheric upwelling velocities associated with the solisticial Hadley cell can be as large as 1 cm s^{-1} (Dima and Wallace 2003), an order of magnitude larger than upwelling velocities in the lower stratosphere. Since the Hadley circulation is closely tied to the meridional gradient of SST (Emanuel 1995), the connection between tropospheric warming and lower stratospheric upwelling is one that perhaps deserves attention.

Observational data suggests there is tight coupling between tropospheric warming and the BDC shallow branch mass flux, at-least when using sea-surface temperature (SST) to characterize the tropical troposphere. On daily to climate change time scales, there is a remarkable anti-correlation between tropical SST and tropopause temperature; these correlations exist on local, regional, and global scales (Fu et al. 2006; Holloway and Neelin 2007; Lin et al. 2015). In general circulation models (GCMs) and reanalyses, there are also strong correlations between tropical mean SST and the BDC shallow branch mass flux, across a wide variety of time scales (Lin et al. 2015; Orbe et al. 2020; Abalos et al. 2021). One of the dominant sources of interannual tropical SST variability is ENSO (El Niño Southern Oscillation), which has been tied to fluctuations in upwelling in the tropical stratosphere (Randel et al. 2009). Interannual variations in tropical mean SST explain 40-50% of the interannual variability of the 70-hPa vertical mass flux (Lin et al. 2015; Abalos et al. 2021). Note, that interannual fluctuations in ENSO-neutral years still exhibit this strong relationship (Lin et al. 2015). In addition, nearly 70% of the CMIP6 model spread in the long-term trend of shallow branch mass flux is explained by the spread in tropical warming (Abalos et al. 2021).

Given the downward-control paradigm, it is no surprise that the tight coupling between tropical SST and BDC shallow branch upwelling on interannual to climate change time scales has been explained through changes to the wave-drag: surface warming leads to upper tropospheric warming and modification of the sub-tropical jets, which can alter the upwards propagation and dissipation of sub-tropical waves (Garcia and Randel 2008; Calvo et al. 2010; Shepherd and McLandress 2011; Lin et al. 2015). While we do not refute the possibility for these mechanisms to be at play, they do not sufficiently explain the ever-present, local scale anti-correlation between SST and tropopause temperature (Fu et al. 2006; Holloway and Neelin 2007). Here, we hope to expand on the idea posed in PE99: can thermal forcing of the troposphere modulate the stratospheric temperature and upwelling?

In this study, we will provide some theoretical evidence for how the geostrophic adjustment of the stratosphere to conditions at the tropopause can directly influence upwelling in the stratosphere. Section 2 uses the linearized quasi-geostrophic potential vorticity equations to show the importance of radiative relaxation in setting the upward penetration of tropopause anomalies. Section 3 shows how anomalies in SST can influence tropical upwelling, using a steady, zonally symmetric, coupled troposphere-stratosphere system. Section 4 uses reanalysis data to argue for the real-world presence of the processes described in the proposed theory. Section 5 concludes the study with a summary and discussion.

2. Stratospheric Response to a Tropopause Anomaly

To first understand how the stratosphere responds to tropospheric forcing, we consider the stratosphere subject to a steady tropopause forcing (i.e. a steady lower boundary condition). Consider the linearized quasi-geostrophic potential vorticity (QGPV) equations on an f-plane:

$$q'(x,y,z) = \frac{1}{f_0}\nabla_H^2\phi' + \frac{f_0}{N^2}\frac{\partial^2\phi'}{\partial z^2} - \frac{f_0}{HN^2}\frac{\partial\phi'}{\partial z} \tag{1}$$

where q is the potential vorticity (PV), f_0 is the Coriolis parameter, N is the buoyancy frequency, ϕ is the geopotential, and H is the scale height. We non-dimensionalize by:

$$\begin{aligned} &x \to Lx \qquad y \to Ly \qquad z \to Hz \\ &\phi \to H^2N^2 \qquad q \to f_0 q \qquad t \to t/f_0 \end{aligned} \tag{2}$$

where $L = NH/f$ is the Rossby radius of deformation. Non-dimensionalizing, dropping primes for perturbation quantities, and assuming wave-like solutions in the zonal and meridional $[\exp(ikx+ily)]$, we obtain

$$L\phi = q(z) \tag{3}$$

where:

$$L = \left(\frac{\partial^2}{\partial z^2} - \frac{\partial}{\partial z} - (k^2+l^2)\right)\phi \tag{4}$$

We consider the boundary conditions that:

$$\phi(z=0) = \phi_T \tag{5}$$

$$\frac{\partial\phi}{\partial z}(z=\infty) = 0 \tag{6}$$

such that the bottom boundary condition represents a steady geopotential forcing at the tropopause, and the upper boundary condition requires the temperature anomaly (or vertical velocity anomaly) be zero.

The general solution to the homogeneous partial differential equation ($q(z) = 0$) is:

$$G(z) = A\exp(m_+z) + B\exp(m_-z) \tag{7}$$

where $m_\pm = 1 \pm \sqrt{1+4(k^2+l^2)}$. Note, since $k^2+l^2 > 0$, $m_+ > 0$ and $m_- < 0$ for all $k > 0$ and $l > 0$.

Next, we define the Green's function, which satisfies

$$LG(z,\xi) = \delta(z-\xi) \tag{8}$$

and is

$$G(z,\xi) = \begin{cases} A\exp(m_+z) + B\exp(m_-z), & \text{for } 0 < z < \xi \\ C\exp(m_+z) + D\exp(m_-z), & \text{for } \xi < z < z_{\text{top}} \end{cases} \tag{9}$$

where z_{top} is assumed to be the top of the domain. The lower boundary condition requires that:

$$A + B = \phi_T \tag{10}$$

and the upper boundary condition requires that:

$$Cm_+\exp(m_+z_{\text{top}}) + Dm_-\exp(m_-z_{\text{top}}) = 0 \tag{11}$$

Note that we choose to explicitly include z_{top} in Equation 11, since numerically evaluating the Green's functions requires $z_{\text{top}} < \infty$. Continuity of G across ξ requires:

$$A\exp(m_+\xi) + B\exp(m_-\xi) = C\exp(m_+\xi) + D\exp(m_-\xi) \tag{12}$$

$$\lim_{\epsilon\to 0}\frac{\partial G}{\partial z}\Big|_{z=\xi-\epsilon}^{z=\xi+\epsilon} - \lim_{\epsilon\to 0} G\Big|_{z=\xi-\epsilon}^{z=\xi+\epsilon} = 1 \tag{13}$$

Equations 10-13 are solved to obtain:

$$A = \frac{\phi_T - \frac{1}{m_d}\left(\exp(-m_-\xi) - \frac{m_+}{m_-}\exp(-m_+\xi + m_d z_{\text{top}})\right)}{1 - \frac{m_+}{m_-}\exp(m_d z_{\text{top}})} \tag{14}$$

where

$$m_d = m_+ - m_- = \sqrt{1+4(k^2+l^2)} > 0 \tag{15}$$

B, C, and D are then obtained using Equations 10, 11, and 12.

First, we look at the stratospheric response to a geopotential anomaly at the tropopause, with zero perturbation PV throughout the rest of the stratosphere (i.e. $q = \delta(\xi)$). Since there is zero perturbation PV throughout the rest of the stratosphere, this can be considered as the fast stratospheric response (geostrophic adjustment) to a tropopause geopotential anomaly. In this classical case, the solution is straightforward; $C = 0$ and $D = 1$, such that:

$$\phi(z) = \exp\left(m_-z\right) \tag{16}$$

where

$$m_- = \frac{1 - \sqrt{1+4(k^2+l^2)}}{2} \tag{17}$$

which shows that m_- scales approximately linearly with the horizontal scale of the tropopause PV anomaly. This also shows that the anomaly decays with a length scale inversely proportional to the horizontal scale of the anomaly. Note that on re-dimensionalization, the Rossby penetration

depth

$$R_d = \frac{f_0 L}{N} \tag{18}$$

where L is the horizontal scale, is the operative vertical scale of the geopotential. As such, tropopause anomalies with large horizontal scales will extend deeper into the stratosphere than smaller ones. However, this means that R_d is quite small in the tropics, but increases with latitude.

It is instructive to convert back into dimensional units to understand the penetrative depth of the tropopause geopotential anomaly, under zero perturbation PV throughout the stratosphere. The geopotential decays to half of its tropopause value at $\ln(2)/|m|$ times the scale height (the non-dimensionalization used in this study). Figure 1 shows the height above the tropopause at which the geopotential decays to half its tropopause value as a function of the horizontal scale, assuming a scale height of $H = 8$ km. Here, we can see that, at-least on fast adjustment time scales, only at the largest scales does the geopotential anomaly extend appreciably into the stratosphere.

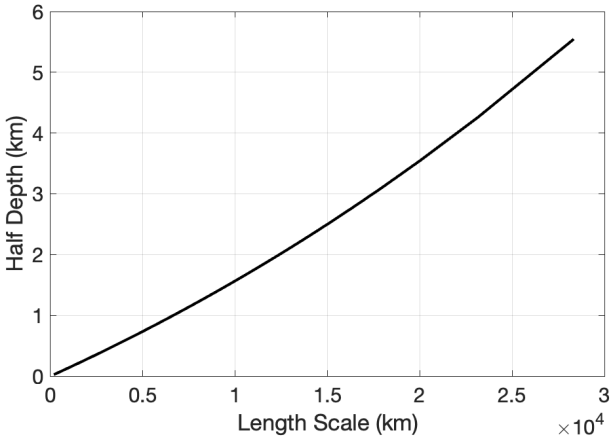

FIG. 1. The height above the tropopause at which the geopotential decays to half its tropopause value, as a function of L, the horizontal length scale (km). The scale height assumed is $H = 8$ km.

Perhaps what is more important than the geopotential anomaly is the temperature anomaly, since the stratosphere is in approximate radiative equilibrium. The temperature anomaly, scaling with $\frac{\partial \phi}{\partial z}$, will also decay exponentially with height. Here, we introduce scaling arguments to further understand the depth and magnitude of temperature anomalies associated with a tropopause geopotential anomaly. Thermal wind balance dictates that

$$g\frac{\partial \ln T}{\partial y} = -f\frac{\partial u}{\partial z} \tag{19}$$

If we take ∂z to scale as the Rossby penetration depth, then we obtain:

$$\ln T \approx \frac{Nu}{g} \tag{20}$$

Note that f drops out, which indicates that the temperature in the stratosphere does not directly depend on f. It rather depends on the magnitude of the tropopause anomaly, as well as the stratospheric stratification. Therefore, perturbations at the tropopause can create large temperature perturbations, though these will be confined to a rather shallow layer near the equator according to the Rossby penetration depth.

Next, it is instructive to consider how the stratosphere responds. As alluded to earlier, temperature anomalies disturb the radiative equilibrium of the stratosphere. This must be associated with radiative heating anomalies. In this case, PV is no longer conserved. The response of the stratosphere to the tropopause geopotential anomaly can be modeled using the classical (dimensional) linearized QGPV equations under thermal forcing:

$$\frac{\partial q}{\partial t} = \frac{f_0}{N^2}\frac{\partial \dot{Q}}{\partial z} \tag{21}$$

where $\dot{Q}$ is the heating rate, and is parameterized to be a simple Newtonian radiative relaxation:

$$\dot{Q} = -\alpha_r \frac{\partial \phi}{\partial z} \tag{22}$$

$\alpha_r > 0$ is the inverse time scale of the Newtonian radiative relaxation. Hitchcock et al. (2010) found that linear radiative relaxation can explain around 80% of the variance in longwave heating rates in a climate model, though this is dependent on the relaxation rate having a height-dependence. Non-dimensionalizing using Equation 2, we obtain:

$$\frac{\partial q}{\partial t} = -\gamma \frac{\partial^2 \phi}{\partial z^2} \tag{23}$$

where $\gamma = \alpha_{\text{rad}}/f_0$. Hitchcock et al. (2010) estimated the radiative relaxation time scale to be approximately 25 days in the lower tropical stratosphere, such that at a latitude of 10°, $\gamma \approx 0.02$, which indicates the slow stratospheric response to the the tropopause geopotential anomaly.

Consider a positive geopotential anomaly at the tropopause. This is initially associated with a cold anomaly in the stratosphere, which radiatively heats and thus rises. If this process is allowed to proceed towards a steady state back to radiative equilibrium, the geopotential must eventually become constant with height (i.e. barotropic), according to Equation 22. This means that temperature anomaly of the equilibrated state is zero. As a result, the PV must be constant throughout the depth of the stratosphere. This can be directly shown using the Green's function solved for earlier. The Green's function can be convoluted with

the source term to solve for the geopotential:

$$\phi(z) = \int_0^\infty G(z,\xi) q(\xi) d\xi \tag{24}$$

This can be done straightforwardly numerically, with z_{top} replacing the upper bound. Before proceeding, we consider the lower boundary condition. For a geopotential anomaly at the tropopause, the associated PV anomaly is:

$$q_T = -(k^2 + l^2)\phi_T \tag{25}$$

This means that a positive geopotential anomaly is associated with a negative PV anomaly. Furthermore, if the geopotential becomes barotropic, then $\phi(z) = \phi_T$. As a result, the tropopause geopotential anomaly determines the barotropic geopotential throughout the entire stratosphere.

Figure 2 shows the stratospheric geopotential solutions that describe the initial and final states of a tropopause geopotential forcing. The initial geopotential distribution from the steady geopotential forcing [i.e. the Green's function with $\delta(z-0)$] is shown as ϕ_b, and is just the zero interior perturbation PV solution mentioned earlier in the text. If the system is allowed to evolve through radiative relaxation to a steady-state, the geopotential becomes barotropic throughout the depth of the stratosphere, which is elicited by ϕ. Here, associated with the barotropic geopotential is also a constant interior PV distribution. The geopotential distribution associated with the generation of anomalous PV through diabatic heating by radiative relaxation is shown in ϕ_q, while the total (barotropic) geopotential is shown as $\phi = \phi_q + \phi_b$. Hence, if given a sufficiently long time to geostrophically adjust to a steady geopotential tropopause forcing, the stratosphere will become barotropic.

At this point, we have said nothing about the relaxation time scale of the stratosphere, which seems to be crucial to this process. If radiation is fast, then the barotropic state can be reached quite quickly. But, if it takes a long time to reach the barotropic state, other unsteady processes may be more important in dictating the state of the stratosphere. It is possible to numerically calculate the amount of time it takes for the system to reach its final barotropic state, by time-stepping Equation 23 forwards in time while holding the lower-boundary PV fixed. For a stratosphere with a depth of around 32-km ($z_{\text{top}} = 4$ for a scale height of $H = 8$ km), assuming $\gamma = 0.02$ and a Coriolis parameter akin to that at 10° latitude, it takes around 3 years for the system to become barotropic. This long equilibration time is a direct consequence of the slow relaxation time scale of radiation in the stratosphere. Note that even for fixed γ and f_0, the total time it takes the (numerical) system to evolve towards the steady-state depends on z_{top}. Regardless, this exercise shows that it takes around an order of a few years for the stratosphere to equilibrate to a tropopause PV forcing (though this might be an overestimate, since radiative relaxation time scale becomes faster as one moves upwards in the stratosphere).

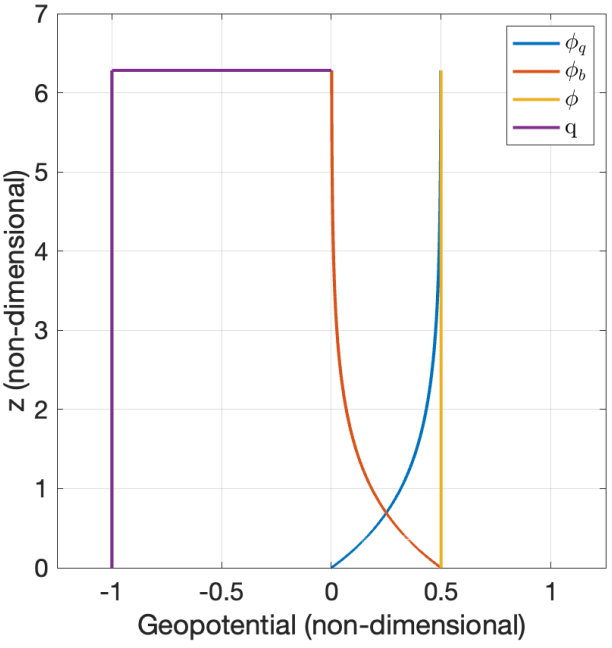

FIG. 2. The geopotential associated with (red) a boundary PV anomaly of $q = -1$ (ϕ_b), (blue) a constant PV anomaly of $q = -1$ in the interior (ϕ_q), and (yellow) the sum of the two ($\phi = \phi_q + \phi_b$). The corresponding total PV is shown in purple. Here we also assume $k = 1$, $l = 1$, and $z_{\text{top}} = 1 + 2\pi$.

This long relaxation time makes it unlikely that the barotropic state is ever reached in the real stratosphere. We believe there are two primary reasons for this. First, wave-drag serves to destroy this equilibration process, since any momentum flux above the upward propagating geopotential anomaly could an overturning circulation through conservation of angular momentum. This will be further explored in the next section. Second, even in the absence of wave-drag, the seasonal cycle would shift the tropopause geopotential anomaly, such that the tropopause forcing shifts latitudinally. Given that it takes on the order of years for the stratosphere to reach a steady, barotropic state, it is unlikely that this final barotropic state will ever be realized in the real atmosphere. However, this would be difficult to judge in any numerical model, since sponge layers are often placed at the top of the stratosphere to dissipate upward propagating waves. The height-dependent dissipation provided by the sponge layer would thus damp the barotropic mode.

Perhaps what is more important, then, are the intermediate states in between the fast, null-stratospheric response [ϕ_b in Figure 2] in which the anomaly decays exponentially with height, and the barotropic steady-state response

in which the boundary anomaly is communicated throughout the depth of the stratosphere [ϕ in Figure 2]. To understand the time scales involved, we numerically integrate the equations forward in time.

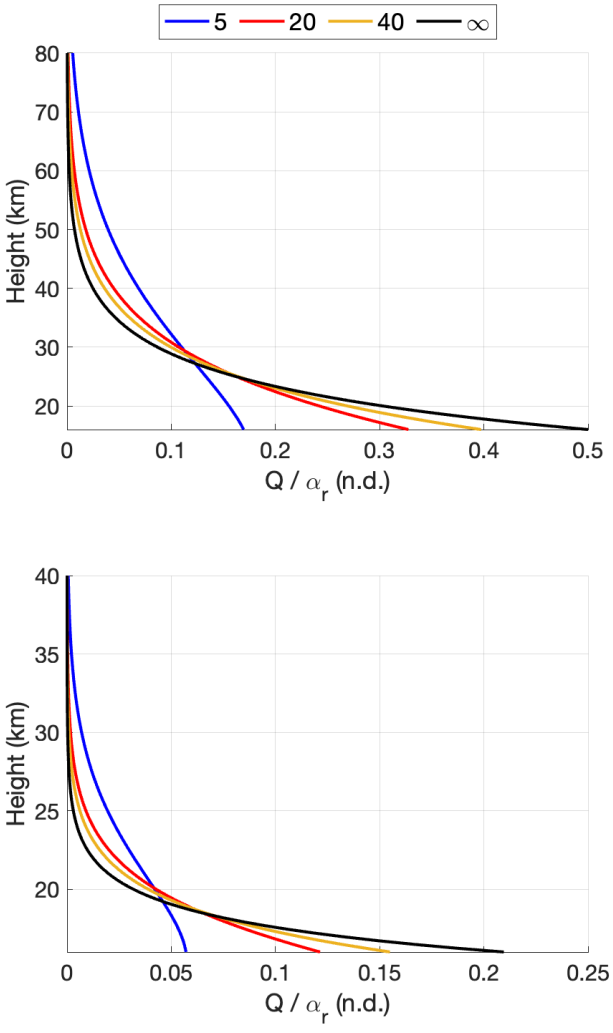

FIG. 3. (Top) The diabatic heating profile (Q/α_r) with height in the stratosphere after 30 days of integration, subject to a steady, $\phi_T = (k^2+l^2)^{-1}$ tropopause boundary forcing of horizontal scale $k = l = 1$, and a (blue) 5-day, (red) 20-day, (yellow) 40-day radiative relaxation time scale. (Bottom) Same as top but for $k = l = 3$. We assume a scale height of $H = 8$ km, and a tropopause height of 16 km to convert to dimensional height.

For practical purposes, the geopotential anomaly is not as important as the associated radiative heating, which is potentially important for tracer transport into the stratosphere. Figure 3 shows the diabatic heating profiles with height after 30 days of integration, for a stratosphere subject to a tropopause geopotential forcing that is associated with a unitary non-dimensional anticyclonic PV, under varying magnitudes of stratospheric radiative relaxation rates. The diabatic heating profiles are normalized by the radiative relaxation rate. We choose 30 days of integration since it is an approximate time scale of the seasonal cycle. For comparison purposes, we show the temperature anomaly associated with the (time-independent) zero perturbation PV geopotential solution (i.e. an infinite radiative-relaxation time scale), even though there is no associated diabatic heating, by definition. Figure 3 shows that after 30-days, there is a non-trivial lifting (in height) of the diabatic heating anomaly over time. The stronger the strength of radiative relaxation, the faster the diabatic heating anomaly is communicated into the stratosphere. We also observe that tropopause anomalies of larger horizontal scale have larger penetrative depths, as expected.

To better understand how radiation modifies the upwards extent of tropopause geopotential anomalies, we define h_d to be the depth at which the geopotential decays to half of its tropopause magnitude (which exists if the system is far from its barotropic state). We also define:

$$h_{d0} = \ln(2)/|m| \tag{26}$$

which is the depth at which the geopotential of the zero-PV stratosphere solution decays to half of its tropopause magnitude ([ϕ_b in Figure 2]). Then, $h_d - h_{d0}$, which always must be greater than zero, is a proxy for the time-dependent, upwards extension of the geopotential anomaly that compared to that if radiative relaxation were to not exist (i.e. the zero interior PV solution).

Figure 4, left, shows $h_d - h_{d0}$ as a function of the integration time (in days), for varying magnitudes of stratospheric radiative relaxation timescales, and for $k = l = 1$. Note that radiative damping time scales in the stratosphere have a significant height dependence, increasing from around 25 days at 100-hPa to around 5 days at 1-hPa (Hitchcock et al. 2010). For a radiative damping time scale of 25 days, akin with that right above the tropopause, we observe that for $k = l = 1$, the geopotential anomaly rises around 2-km in 25 days, and around 6-km in 90 days. Note that for $k = l = 1$, $h_{d0} \approx 5.5$ km (see Figure 1). For $k = l = 3$, $h_{d0} \approx 1.5$ km, eliciting the much shallower penetration of the tropopause geopotential anomaly into the stratosphere for smaller scale anomalies. However, with the addition of $\alpha_r = 25$ days, the geopotential anomaly rises a distance h_{d0} in around two months. Therefore, radiative relaxation plays a much larger role in communicating a tropopause geopotential anomaly upwards into the stratosphere for smaller horizontal disturbances than large ones.

There is a relatively simple physical explanation for the processes that are occurring here. A tropopause geopotential anomaly elicits a vertically shallow response in the tropical stratosphere, as illuminated by the zero-perturbation-PV solutions in the stratosphere. However, radiative relaxation wants to smooth out the temperature anomalies associated with tropopause geopotential anomaly. If the

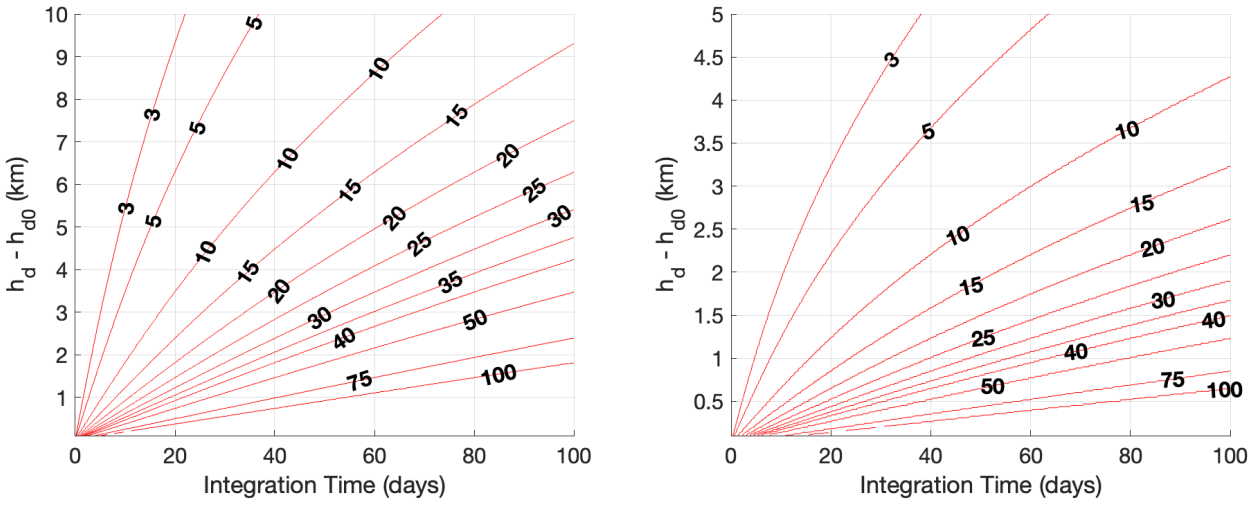

FIG. 4. $h_d - h_{d0}$, or the increase in the depth (km) at which the geopotential reaches half of its tropopause anomaly, as a function of integration time (days). Contours are labeled by the constant radiative relaxation time scales (days). A scale height of 8-km, $f = 2\Omega\sin(10°)$, (left) $k = l = 1$ and (right) $k = l = 3$ is assumed.

tropopause geopotential anomaly is steady, the only way to achieve radiative equilibrium is to adjust the geopotential such that it becomes constant with height. Here, we stress that the geopotential does not have to go to zero, as in Holloway and Neelin (2007). The only requirement is that the energy density goes to zero (which it does if ϕ is constant with height). This process, however, takes on the order of a few years, owing to the slow time scale of radiation in the stratosphere. Thus, one would undoubtedly question whether the tropopause geopotential anomaly can indeed be steady over these long time scales. Our calculations of the relatively idealized, time-dependent case shows that radiation still plays a significant role in lifting the geopotential anomaly and creating PV in the stratosphere, even if the final barotropic state is unlikely to be achieved in the real atmosphere.

3. Troposphere-Stratosphere Response to SST

In the previous section, we used a simple QGPV framework to understand how a tropopause geopotential anomaly affects the stratosphere, using the tropopause as a lower boundary condition for the stratosphere. In reality, however, the tropopause and stratosphere are coupled. In this section, we develop a simple coupled troposphere-stratosphere model to directly show how SST anomalies can induce responses in the stratosphere, and explore how radiation and wave-drag can modulate these responses.

a. Model Formulation

Lin and Emanuel (2022) formulated a linear, coupled troposphere-stratosphere model, but in the context of unsteady equatorial waves. In that linear system, a convecting, quasi-equilibrium troposphere was coupled to a dry and passive stratosphere. We use the same system derived in Lin and Emanuel (2022), except we only consider steady circulations, governed by:

$$-\frac{\partial \phi_0}{\partial x} + yv_0 - F(u_0+u_1) = 0 \tag{27}$$

$$-\frac{\partial \phi_0}{\partial y} - yu_0 = 0 \tag{28}$$

$$\frac{\partial s^*}{\partial x} + yv_1 - F(u_0+u_1) - Du_1 = 0 \tag{29}$$

$$\frac{\partial s^*}{\partial y} - yu_1 = 0 \tag{30}$$

where u_0 and v_0 are the barotropic zonal and meridional winds, u_1 and v_1 are the baroclinic zonal and meridional winds, ϕ_0 is the barotropic geopotential, s^* is the saturation moist entropy (that is assumed to be vertically constant, as in a quasi-equilibrium troposphere), F is the non-dimensional surface friction coefficient, and D is a non-dimensional passive "wave-drag", i.e. drag that responds solely to the flow. In the ensuing text, terms with an overlying hat are dimensional. $\hat{D}$, the (dimensional) inverse time scale of the linear Rayleigh damping by wave-drag, is:

$$\hat{D} \to \frac{\beta L_y^2}{a} D \tag{31}$$

where L_y is the meridional length scale, β is the meridional gradient of the Coriolis force, and a is the radius of the Earth. Here, note that while the passive wave-drag is not meant to be realistic, it is necessary to sustain zonally sym-

metric meridional overturning simulations in the absence of surface friction. Note that while there are equations for the tropospheric thermodynamics in Lin and Emanuel (2022), they are omitted here. In this study, we instead consider a fixed s^*, representative of a SST forcing, since s^* is assumed to be constant with height (quasi-equilibrium) (Emanuel 1987).

We also include a model for the stratosphere. The stratosphere is formulated in log-pressure coordinates and assumed to be in hydrostatic balance. The steady, non-dimensional equations are summarized below:

$$-\frac{\partial \phi_s}{\partial x} + y v_s - D u_s = 0 \tag{32}$$

$$-\frac{\partial \phi_s}{\partial y} - y u_s = 0 \tag{33}$$

$$\frac{\partial u_s}{\partial x} + \frac{\partial v_s}{\partial y} + \frac{1}{\rho_s}\frac{\partial (\rho_s w_s^*)}{\partial z^*} = 0 \tag{34}$$

$$w_s^* S = -\alpha_{\rm rad}\frac{\partial \phi_s}{\partial z} \tag{35}$$

$$\rho_s = \exp\left(\frac{H}{H_{s,s}}(1-z^*)\right) \tag{36}$$

where subscripts of s denote quantities in the stratosphere, w_s^* is the log-pressure vertical velocity, S is a non-dimensional stratospheric stratification, ρ_s is the basic state density, H is the dimensional tropopause height, $H_{s,s}$ is the dimensional scale height in the stratosphere, $\alpha_{\rm rad}$ is the non-dimensional radiative damping time scale in the stratosphere, and the log-pressure vertical coordinate $z^* \equiv -H\ln(p/p_t)+1$ is defined such that $z^*=1$ is the bottom boundary, or the tropopause. Note that a passive wave-drag, D, is also included in the stratosphere. S plays an important role in the behavior of this model, and is:

$$S = \frac{N^2 H^2}{\beta^2 L_y^4} \tag{37}$$

where N is the buoyancy frequency. For $N^2 = 6\times10^{-4}$, $H =$ 16 km, $\beta = 2.3\times10^{-11}$, and $L_y = 1200$ km (such that $y=1$ represents approximately ten degrees of latitude), $S \approx 150$. For a dimensional $\hat{\alpha}_{\rm rad} = 30$ days^{-1} radiative damping time scale in the stratosphere, the non-dimensional radiative relaxation in this model is:

$$\hat{\alpha}_{\rm rad} = \frac{\beta L_y^2}{a}\alpha_{\rm rad} \approx 0.07 \tag{38}$$

b. Stratospheric response to tropopause forcing

Here, we consider zonally symmetric circulations. In this case the stratospheric equations can be reduced to a single differential equation for the geopotential:

$$\frac{\partial^2 \phi}{\partial z^2} - \frac{H}{H_{s,s}}\frac{\partial \phi}{\partial z} + \frac{\xi}{y^2}\left[\frac{\partial^2 \phi}{\partial y^2} - \frac{2}{y}\frac{\partial \phi}{\partial y}\right] = 0 \tag{39}$$

where

$$\xi = \frac{DS}{\alpha_{\rm rad}} = \frac{\hat{D}S}{\hat{\alpha}_{\rm rad}} \tag{40}$$

is a non-dimensional term that depends on the ratio between the time scale of wave-drag to that of radiation. When the radiative time scale is much faster than the wave-drag time scale ($\xi << 1$), the meridional derivative terms are small and the system will become nearly barotropic in the vertical. On the other hand, when the wave-drag time scale is much faster than the radiative time scale ($\xi >> 1$), the tropopause anomaly will not extend very far into the stratosphere. This is qualitatively similar to the properties shown in the simple QGPV model in the previous section. Note that on Earth, $S \sim O(10^2)$, such that $\xi = 1$ when the wave drag time scale is two orders of magnitude smaller than that of radiation.

Equation 39 can be solved numerically, discretizing the grid in the meridional and vertical directions. The stratospheric geopotential is also subject to a zero temperature anomaly at the top of the domain, or equivalently, zero derivative of the geopotential. The geopotential anomaly is enforced to be zero on the northern and southern borders. For illustrative purposes, we first solve the equations under a fixed lower boundary condition:

$$\phi(z^*=1) = \phi_T \tag{41}$$

where

$$\phi_T = \int_y y\exp\left(-((y-2)/2)^2\right) - y\exp\left(-((y+2)/2)^2\right) \tag{42}$$

This represents a flat geopotential anomaly in the tropics that decays to zero in the subtropics. As will become clear later when the solutions are coupled to the troposphere, this geopotential structure is associated with sub-tropical jets at $y = \pm 2$.

Figure 5 shows the stratospheric response to a tropopause geopotential anomaly, under varying values of ξ. Here, the numerical calculations confirm the mathematical analysis. Indeed, for $\xi = 0.1$ (i.e. when wave-drag is very weak), radiation acts to create a nearly barotropic stratosphere, in which motion is confined to constant angular momentum surfaces. The vertical structure of the vertical velocity in this case is qualitatively similar to the thermally forced vertical mode calculated in PE99 [see their Fig. 11]. When the time scale of wave-drag is faster than radiation ($\xi = 100$), the vertical penetration of the tropopause geopotential anomaly is significantly muted. In fact, the vertical velocity anomalies only extend on the

order of a few km into the stratosphere. In this sense, wave-drag acts to both mute the vertical scale of the tropopause geopotential anomaly, and sustain a meridional overturning circulation. Thus, what this analysis highlights is that the stratospheric response to a tropopause geopotential anomaly is not only a function of the strength of wave drag, but also a function of the strength of radiative relaxation in the stratosphere.

c. Tropospheric forcing of stratospheric upwelling

Next, we couple the stratospheric equations to the zonally symmetric tropospheric equations, to show how tropospheric thermal forcing can influence stratospheric upwelling. In order to couple the troposphere and stratosphere, we use classical matching conditions: (1) continuity of pressure (geopotential) and (2) vertical velocity at the tropopause:

$$\phi_s(z^* = 1) = \phi_T \tag{43}$$

$$B\omega(\hat{p}_T) = -w_s^*(z^* = 1) \tag{44}$$

where $\hat{p}_T$ is the non-dimensional tropopause pressure, and B is a scaling coefficient between pressure velocity and vertical velocity (as in Lin and Emanuel (2022))

$$B = \frac{H_{s,t}}{H}\frac{p_s - p_t}{p_t} \tag{45}$$

Here, p_s is the surface pressure, p_t is the tropopause pressure, and $H_{s,t}$ is the scale height of the troposphere. Note that B indirectly depends on the dry stratification of the troposphere. Using these coupling conditions leads to an equation for u_0:

$$u_0 = -y\gamma \int_y \frac{\partial \phi_s}{\partial z^*}\Big|_{z^*=1} dy - \frac{1}{y}\frac{\partial s}{\partial y} \tag{46}$$

where

$$\gamma = \frac{\alpha_{\text{rad}}}{FSB} \tag{47}$$

is an additional non-dimensional parameter that qualitatively represents the strength of troposphere-stratosphere coupling. Note that it is not entirely independent from ξ. Here we see that under a rigid lid condition, $S \to \infty$, $\gamma = 0$, such that the barotropic mode becomes only a function of the tropospheric forcing. In addition, B is proportional to the troposphere scale height, which itself is inversely proportional to the buoyancy frequency. Hence, SB can also be thought of as a scaled ratio of the troposphere buoyancy frequency to the stratosphere buoyancy frequency. Curiously, the strength of radiative relaxation appears in the numerator of γ. This is because the strength of radiative relaxation determines the magnitude of the vertical velocities (which balance temperature anomalies) in the stratosphere. In this way, stratospheric radiative relaxation can force the barotropic mode in a "top-down" fashion. This analysis shows that the tropospheric barotropic mode depends on not only the tropospheric SST anomaly, but also on the stratospheric geopotential at the tropopause. This is reasonable, as the tropospheric barotropic mode is associated with non-zero tropopause vertical velocity anomalies; as such, the magnitude of the barotropic mode is expected to be controlled by both tropospheric and stratospheric processes.

We proceed by numerically solving the troposphere and stratosphere equations. In order for the continuity of pressure to be satisfied, the geopotential boundary condition must satisfy:

$$\phi_T = \phi_0 - V_1(\hat{p}_t)s^* \tag{48}$$

where $V_1(p_t)$ is the non-dimensional baroclinic mode magnitude evaluated at the tropopause pressure p_t (Lin and Emanuel 2022):

$$V_1(p) = \frac{\overline{T}(p) - [\overline{T}]}{T_b - [\overline{T}]} \tag{49}$$

Here, $\overline{T}$ is the basic-state temperature of the troposphere, $[\overline{T}]$ is the basic state vertically-averaged temperature, and T_b is the basic state boundary layer temperature. Hence, $V_1(p_t)$ is negative. Note that the geopotential is the linear sum of the contributions of the tropospheric barotropic and baroclinic modes.

Solving for the stratosphere in isolation is not possible since ϕ_0 is a function of both the troposphere and stratosphere. In order to also enforce continuity of vertical velocity across the tropopause boundary, we iteratively solve for the stratospheric geopotential. Given a guess for u_0, Equation 28 can be used to to obtain ϕ_0. This then allows for Equation 48 to set the lower boundary condition (ϕ_T) when solving for the geopotential in the stratosphere (Equation 39). The updated stratospheric geopotential is then used to update the solution for u_0 via Equation 46. The iterative process converges quickly (less than 5 iterations) for all of our solutions

We consider a zonally symmetric SST forcing. We observe from Equation 30 that:

$$s^* = \int y u_1 \, dy \tag{50}$$

such that we can specify the baroclinic wind response to obtain a suitable s^* anomaly. Here, we specify:

$$u_1(y) = -\exp\left(-4(y-2)^2\right) - \exp\left(4(y+2)^2\right) \tag{51}$$

which is akin to subtropical jets symmetric about the equator. Note, that under no surface friction ($F = 0$), the merid-

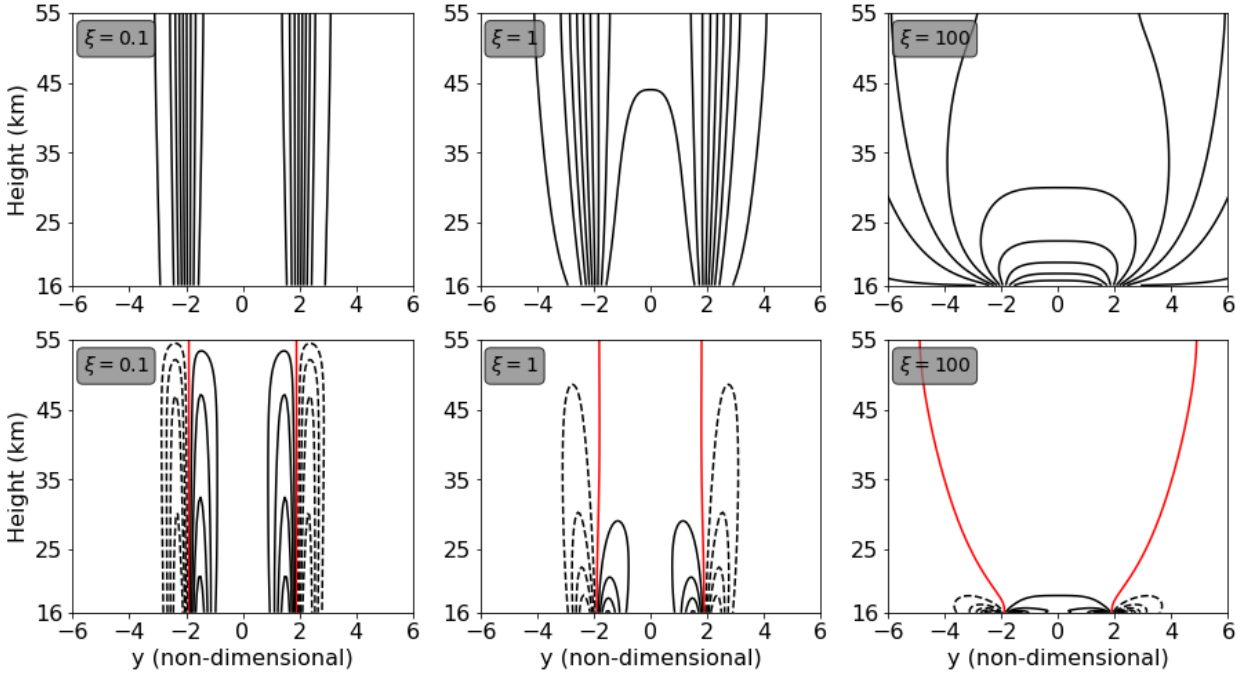

FIG. 5. (Top-row) The zonally symmetric geopotential response to a tropopause geopotential forcing, as shown in Equation 42, for varying values of ξ. (Bottom-row) Same as the top-row except for the zonally symmetric vertical velocity response. The red-line is the zero vertical velocity isoline. The tropopause is defined at 16-km, and a scale height of 7-km is used.

ional baroclinic wind is:

$$v_1 = \frac{D}{y^2}\frac{\partial s^*}{\partial y} \tag{52}$$

This means that the meridional derivative of s^* must go to zero faster than y^{-2} otherwise v_1 will become unstable. Thus, $u_1(y)$ is chosen to satisfy this constraint. Lastly, we use "Earth-like" non-dimensional parameters of $\xi = 25$ and $\gamma = 0.001$. Here, we emphasize that while $S = 150$, $\hat{\alpha}_{\text{rad}} = 30$ days^{-1}, $B = 4.5$, and $F = 0.1$ are estimated for Earth via the non-dimensional scalings, we have chosen the damping time scale of radiation to be approximately half a year, or $\hat{D} = 180$ days^{-1}. This is a relatively weak force, but faster than the 500 days^{-1} time scale used in PE99 to mimic diffusion. Here, our intention is to explore the non-dimensional space of the system, rather than place an exact order of magnitude estimate of tropical wave-drag. However, the importance of even small magnitude terms in the momentum budget in the tropical free atmosphere, akin to the diffusive term in PE99, cannot be overstated.

Figure 6 shows the zonally symmetric, linear response to the prescribed, equatorially symmetric SST forcing, for $\xi = 25$ and $\gamma = 0.001$. We observe a meridionally shallow, thermally direct overturning circulation in the troposphere, associated with sub-tropical jets at $|y| = 2$ that decay exponentially with height into the stratosphere. The tropopause geopotential is elevated in the tropical region ($|y| < 2$), since s^* is assumed to be constant with height (not shown). Associated with this elevated tropopause geopotential is a weak, thermally indirect overturning circulation in the stratosphere. This circulation is also meridionally shallow. Note that the tropospheric thermally direct overturning circulation in this model is not meant to realistically mimic the Hadley circulation, since linear models do not capture the dynamics of the Hadley circulation (Held and Hou 1980). Rather, its purpose in this model is to understand how tropopause geopotential anomalies associated with tropospheric circulations influence upwelling in the stratosphere.

Figure 7 shows the vertical profile of anomalous geopotential and vertical velocity at different meridional points in the linear solution, for varying values of ξ (and γ). We first observe that for all of the values of ξ, the geopotential anomaly maximizes at the tropopause. These positive geopotential anomalies decay as one moves upwards into the stratosphere, but the rate at which they decay is determined by ξ. As shown in the previous section, smaller values of ξ (radiation dominates) lead to a slower decay of ϕ in the stratosphere. For the "Earth-like" case where $\xi = 25$, we also observe almost purely moist-adiabatic vertical velocity profiles in the region of maximum tropospheric upwelling ($y = 1.5$). However, the vertical velocity does

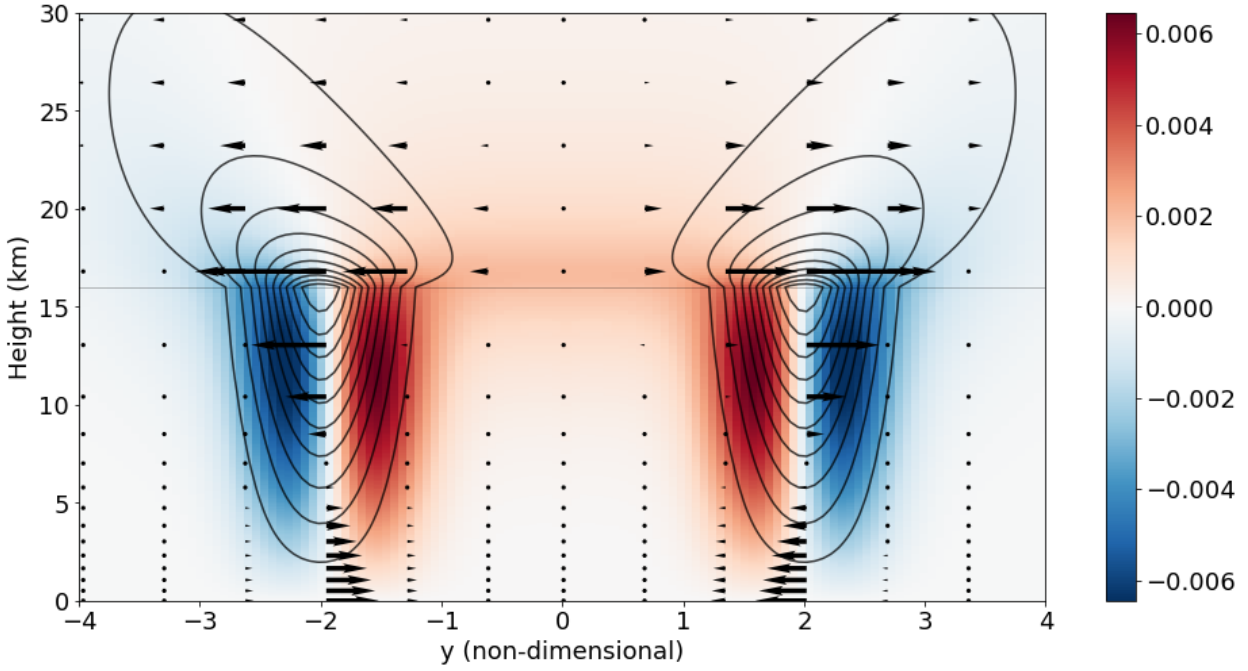

FIG. 6. The zonally symmetric response to the s^* forcing shown in Equation (50). Zonal winds are shown in contours, colors show vertical motion (red for upwards, blue for downwards). Arrows show the meridional motion. The tropopause is shown by the gray line. Earth-like parameters of $\xi = 25$, $\gamma = 0.001$ are used.

not go to zero at the tropopause. Rather, the vertical velocity decays exponentially with altitude in the stratosphere; in the tropical lower stratosphere, the upwelling velocities are an order of magnitude smaller than the peak upwelling velocities in the troposphere. This is what is approximately observed in the real world. These solutions are especially unlike the linear solutions computed by PE99, who found stratospheric upwelling nearly comparable in magnitude to that of the troposphere when the stratosphere was perturbed through tropospheric thermal forcing. As ξ decreases (to values of radiative damping that are greater than observed in the real stratosphere), the magnitude of stratospheric vertical velocities increases to the same order of magnitude as the troposphere. On the other hand, when ξ increases, the vertical penetration of the tropospheric thermal forcing dramatically decreases, to where there is no influence on the stratosphere.

The vertical shape of the geopotential profiles also allows for an estimate of the magnitude of tropopause temperature anomalies per degree of warming in the troposphere. In the troposphere, we see a canonical moist-adiabatic temperature profile (as by definition), with warmer anomalies in the upper troposphere per degree of warming in the boundary layer. For the “Earth-like" case, we observe that the temperature anomalies just above the tropopause are approximately twice the magnitude of the boundary layer anomalies, which is approximately what is observed in convecting regions of the tropical atmosphere (see Fig. 5 in Holloway and Neelin (2007)). The derivative of the geopotential is discontinuous across the tropopause in this model, however, since we assume a discontinuous transition between quasi-equilibrium thermodynamics in the troposphere, and dry, passive dynamics in the stratosphere. In reality, the TTL serves as the interface between the troposphere and stratosphere (Fueglistaler et al. 2009). Thus, one might expect the temperature anomalies to be smoothed out across the transition layer, though further analysis of this will be the subject of future research.

These theoretical results provide a potential explanation for the observed correlation between tropical-averaged SST anomalies and tropical stratospheric upwelling (Lin et al. 2015), as well as the anti-correlation between SST and tropopause temperature (Holloway and Neelin 2007; Fu et al. 2006). First, an SST anomaly is communicated throughout the depth of the troposphere through moist convection. Indeed, observations have found strong positive correlations between the tropopause geopotential anomaly and the boundary layer temperature anomaly (Holloway and Neelin 2007). The tropopause geopotential anomaly at the tropopause is initially associated with cold temperature anomalies just above the tropopause. The strength of radiative relaxation then determines the time scale at which

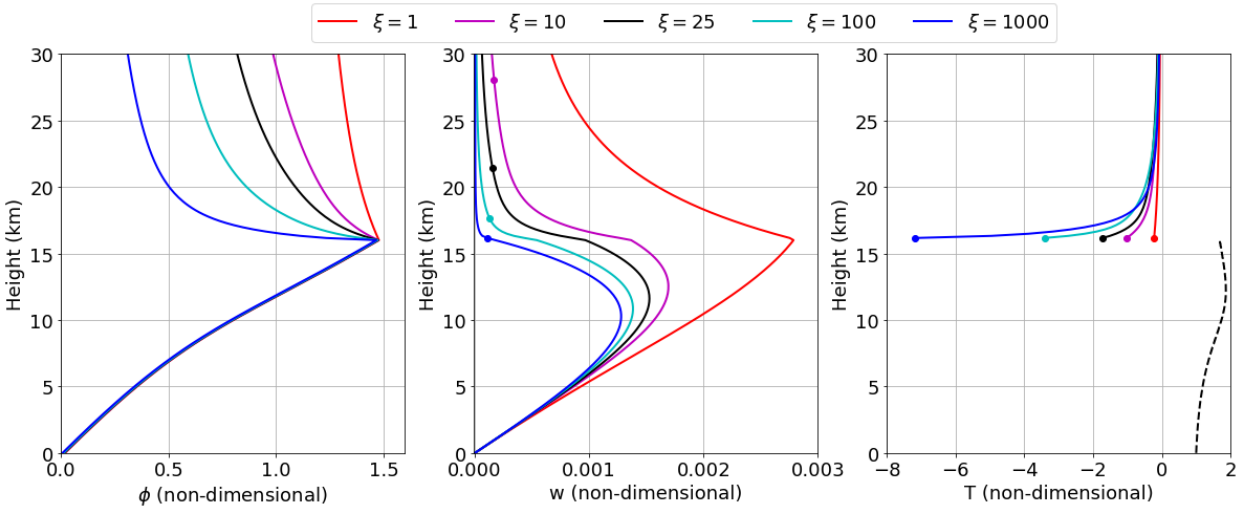

FIG. 7. Vertical profiles of non-dimensional (left) geopotential, (middle) vertical velocity, and (right) temperature at y = 1.5, for varying values of ξ, obtained by varying α_{rad}. Circles in middle panel show where w decays to an order of magnitude smaller than the maximum column w. Profiles are normalized to a 1 degree anomaly in the boundary layer.

the geopotential anomaly rises in the stratosphere through diabatic heating. However, the presence of wave-drag, through conservation of angular momentum, disrupts this process and induces a meridional overturning circulation that mediates the vertical scale at which the geopotential anomaly can rise in the stratosphere. Our work shows that the ratio between the strength of radiative relaxation and that of wave-drag is what determines this penetrative depth, and ultimately, the ability of the troposphere to influence stratospheric tropical upwelling. A number of other quantities are also important. The tropospheric & stratospheric stratification, as well as the shape and length scale of the SST perturbation (L_y), also factor into the non-dimensional parameters that control the vertical decay scale of tropopause geopotential anomalies. In general, large horizontal scale anomalies have a larger penetrative depth into the stratosphere, and thus can more efficiently influence upwelling in the stratosphere than anomalies with smaller horizontal scales. While our analysis in this section was restricted to zonally symmetric circulations, smaller scale geopotential anomalies, such as those imposed by mesocale convective systems or tropical cyclones, can still significantly influence stratospheric upwelling.

4. Tropopause forcing in reanalysis data

In this section, we evaluate the proposed theory using the ERA5 re-analysis product (Hersbach et al. 2019b,a). We use monthly fields of SST, geopotential, and temperature, over the years 1979-2021. Anomalies in all fields are generated by subtracting the linear trend in each field, as well the seasonal cycle.

To begin, we regress the tropical-averaged geopotential, at different vertical levels, onto tropical-averaged SST. Figure 8, solid lines, shows the coefficients of the linear regressions of geopotential and temperature onto SST. We first observe an approximate moist-adiabatic structure in the tropical tropospheric geopotential, consistent with quasi-equilibrium and the findings of previous studies (Holloway and Neelin 2007). We also see large correlations ($r \approx 0.75$) between both tropical-averaged SST and the corresponding 100-hPa geopotential. The coefficient magnitudes and correlations decay with increasing height in the stratosphere, but are still significant and non-negligible even at 50-hPa. Here, we emphasize that the geopotential decay with height (log-pressure) in the stratosphere is not exponential. These findings are in agreement with the processes described in the theory, which predict a similar structure in the geopotential (c.f. Figure 7). Note, for a pure baroclinic mode anomaly, the surface geopotential would be anti-correlated with the upper troposphere anomaly. Thus, in regions where the surface geopotential correlation with SST is positive, there is a significant barotropic component to the geopotential profile associated with SST warming, highlighting the role of the stratosphere.

As in Holloway and Neelin (2007), the temperature structure of the tropical troposphere is approximately moist-adiabatic. Most notably, in all of the regions, the temperature at or above the tropopause is strongly anti-correlated with surface temperature. As stated earlier, we observe tropopause temperature anomalies approximately two times larger in magnitude than that of the surface. The cold anomaly associated with the tropical-averaged SST warming maximize above the geopotential

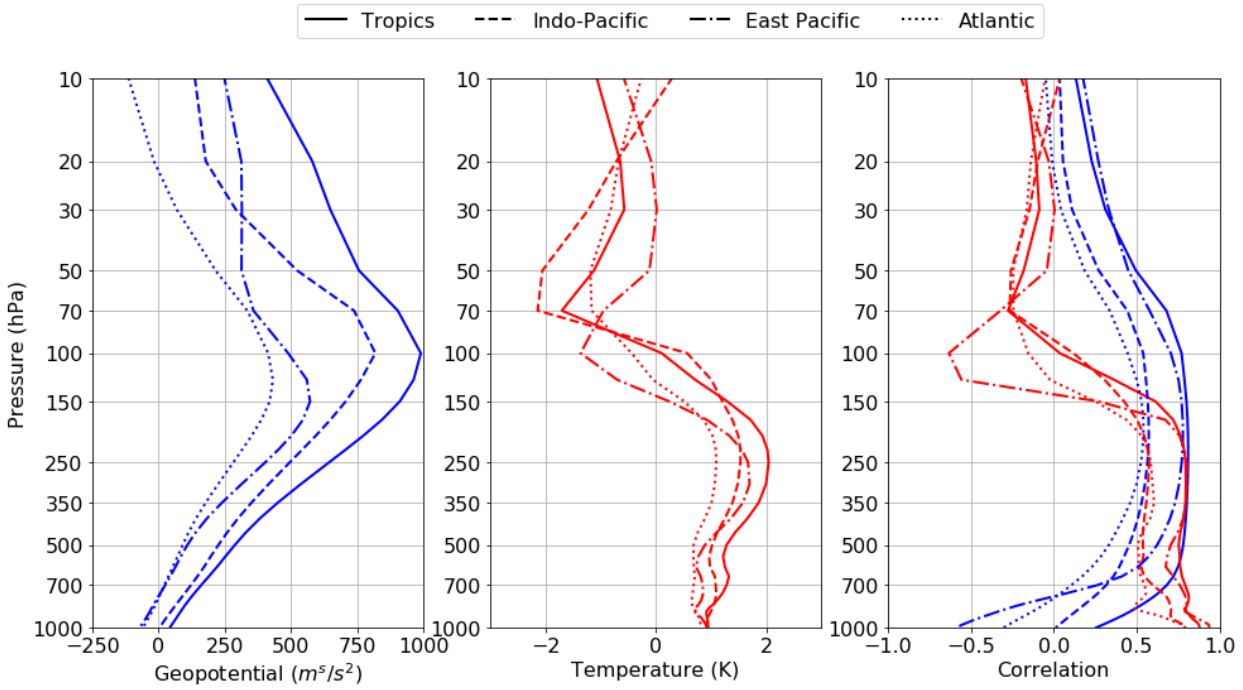

FIG. 8. (Left) Linear coefficient of geopotential at varying levels, regressed onto regionally-averaged SST anomaly. (Middle) Same as the left panel but for temperature. (Right) Vertical dependence of the correlation coefficients for (blue) geopotential and (red) temperature. The regions are (solid) the entire tropics [20°S - 20°N], (dashed) the Indo-Pacific region [(45°E-20°E], (dot-dashed) the East Pacific region [180°E-280°E], and (dotted) the Atlantic region [60°E-0°]. Vertical level is scaled as the logarithm of pressure.

maximum, which is interpreted to occur at the tropical-averaged tropopause.

This analysis is not definitive proof that geostrophic adjustment of the stratosphere to tropopause forcing is a significant process in the lower stratosphere. After all, if stratospheric temperature is modulated by tropical heating through changes to wave-drag (Garcia and Randel 2008; Calvo et al. 2010; Lin et al. 2015), then one would also expect the geopotential to decay with height in the stratosphere, as is shown in Figure 8. Perhaps what is more compelling evidence for the processes described in this study is that the same relationships are also observed on regional scales (the Indo-Pacific, East Pacific, and the Atlantic), as shown in Figure 8. The geopotential anomalies maximize at 100-hPa in the Indo-Pacific, at 125-hPa in the Atlantic, and at 150-hPa in the East Pacific. Thus, the level at which the geopotential anomaly maximizes (interpreted as one measure of the tropopause) is influenced by the mean SST of the region (Held 1982). Most importantly, in each of the regions, the cold anomaly associated with SST warming maximizes above the level of maximum geopotential (as dictated by hydrostatic balance, though this is not strictly enforced in reanalysis). In fact, the regional scale geopotential anomalies persist upwards to at-least 10-hPa, though the correlations drop significantly in magnitude. This means that regional and local scale variations in the lower stratospheric geopotential are strongly influenced by the tropopause geopotential in the same region. This is consistent with the proposed theory, which predicts the existence of correlations between tropospheric geopotential and lower stratospheric geopotential not only on tropics-wide scales, but also on local and regional scales.

In the tropics, the surface temperature need not always be connected to tropospheric warming, especially if the moist static energy of the boundary layer is lower than that of the overlying free troposphere. This is possible since temperature gradients in the tropical atmosphere are weak, owing to the smallness of the Coriolis force, such that convecting regions more effectively modulate the free tropospheric moist static energy (Sobel and Bretherton 2000). To further investigate the influence of tropospheric geopotential on stratospheric geopotential, we show in Figure 9 correlation maps between the 500-hPa geopotential, a proxy for tropospheric heating, and the geopotential at various vertical levels in the lower stratosphere.

In Figure 9, we find that 500-hPa geopotential is an excellent predictor of both the tropopause ($r \approx 0.9$) and lower stratospheric geopotential, though the correlations decrease with increasing height in the stratosphere. This is to be expected, as the vertical penetration of tropopause

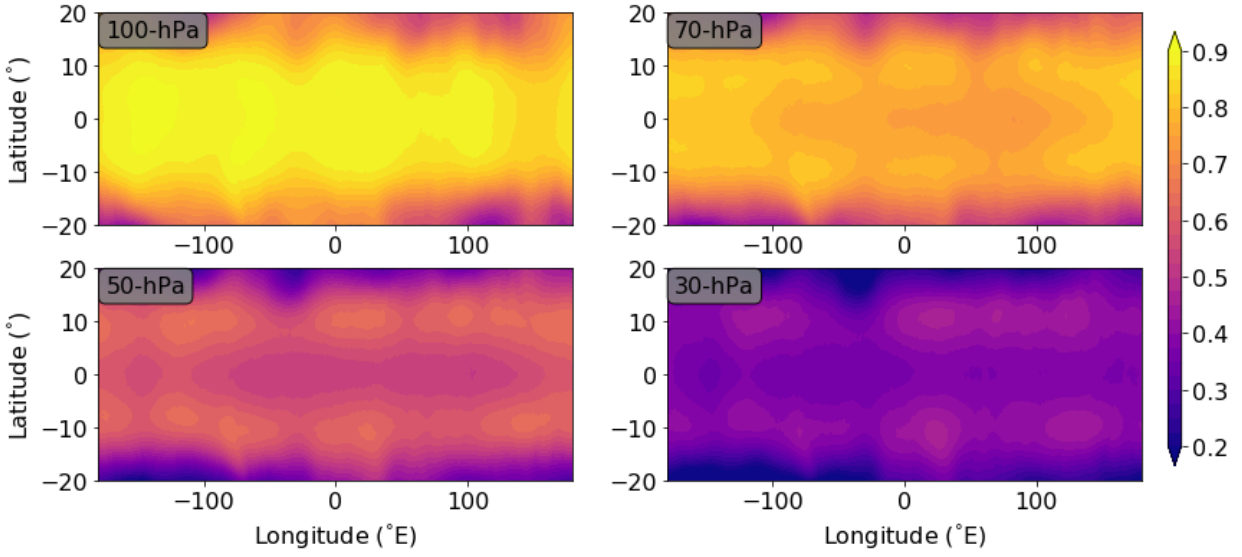

FIG. 9. Correlation of the (top-left) 100-hPa, (top-right) 70-hPa, (bottom-left) 50-hPa, and (bottom-right) 30-hPa anomalous geopotential with the 500-hPa anomalous geopotential.

geopotential anomalies is shallow (though not insignificant), given the slow radiative relaxation in the stratosphere. Regardless, these figures show that monthly 500-hPa geopotential anomalies, even on a grid-point by grid-point basis, are highly correlated with monthly anomalies of 100-hPa geopotential (and upwards in the stratosphere). Interestingly, the magnitude of the geopotential correlations at 100-hPa are largest at the equator. However, the correlation magnitudes move to become the largest off-equator (around 10° latitude), which is most clearly seen in the maps of the 500-hPa geopotential correlation with either 50-hPa or 30-hPa geopotential. These characteristics could be a manifestation of the Rossby penetration depth's dependence on the Coriolis parameter. In other words, tropical geopotential anomalies at the equator have a much smaller vertical penetration than those off the equator.

The analyses shown here suggest that changes in the 500-hPa geopotential are not only associated with changes in the tropopause/lower stratospheric geopotential at zonally-symmetric scales, but also at regional and local scales. Therefore, these simple results provide compelling evidence that the stratosphere undergoes geostrophic adjustment to tropopause forcing. In particular, the regional and local scale correlations are not particularly well explained by theories of wave-drag, which by definition, relate zonally-symmetric tropospheric heating to zonally-symmetric stratospheric temperature. What is clear, however, is that the heights at which upward propagating waves can force the mean circulation are not limited to vertical levels near the wave forcing. The opposite is true for geopotential anomalies at the tropopause; the proposed theory shows that the geopotential anomalies decay with height, such that their influence is limited to levels near the tropopause. In this manner, wave-driving can act as a more effective force as compared to tropopause geopotential forcing in the middle stratosphere, as opposed to the lower stratosphere.

5. Summary and discussion

In this work, we present theoretical evidence for how tropopause geopotential anomalies (generated through tropospheric thermal forcing) can induce upwelling in the stratosphere. Using the linearized QGPV equations, we show that while tropopause geopotential anomalies in the tropics have vertically shallow structures, radiative relaxation (diabatic heating) in the stratosphere acts to increase the vertical penetration of these anomalies. In particular, planetary scale geopotential anomalies can propagate upwards on the order of a few kilometers in a month, such that their vertical penetration is large enough to impact the shallow branch of the Brewer-Dobson circulation. In the steady-state limit, where radiative equilibrium is again satisfied, the stratospheric PV becomes barotropic. Integration of the linearized QGPV equations under realistic radiative relaxation rates in the stratosphere and a steady tropopause anomaly shows that it takes on the order of years for the stratosphere to reach a barotropic state, which is unlikely to be achieved in the real atmosphere.

We then formulate a troposphere-stratosphere linear β-plane model, which couples a convecting troposphere to a dry and passive stratosphere. Under zonally symmetric circulations, we show that the stratospheric response to

tropospheric forcing is controlled by two non-dimensional parameters: (1) ξ, which represents the ratio between the time scale of wave-drag to that of radiation, multiplied by a non-dimensional stratospheric stratification, and (2) γ, which qualitatively represents the strength of troposphere-stratosphere coupling, and is a function of the ratio of the tropospheric buoyancy frequency to the stratosphere buoyancy frequency. We show that in the limit that radiation is much stronger than wave drag, the stratospheric response to a tropopause forcing asymptotically becomes barotropic, while in the opposite limit, the vertical length scale of the tropopause forcing becomes extremely small. Under "Earth-like" values of the non-dimensional parameters, the model predicts that in response to a thermally direct, zonally symmetric tropospheric overturning circulation, there is upwelling in the lower tropical stratosphere that is around an order of magnitude smaller than that of the tropospheric circulation.

The widely accepted theory of tropical stratospheric upwelling is that it is mechanically driven by sub-tropical wave-drag (Haynes and McIntyre 1987; Plumb and Eluszkiewicz 1999). There is ample evidence from numerical modeling suggesting that wave-drag is the dominant mechanism that drives mean and interannual upwelling in both the lower stratosphere and TTL (Boehm and Lee 2003; Norton 2006; Calvo et al. 2010; Ryu and Lee 2010; Gerber 2012; Ortland and Alexander 2014; Kim et al. 2016; Jucker and Gerber 2017, among many others). Of course, it is theoretically impossible to have flow across angular momentum contours without some local drag. We emphasize that in no way does this work attempt to disprove the role sub-tropical wave drag has in modulating tropical stratospheric upwelling. In this model, even though wave-drag purely acts as a passive response to the system, as in the linear system described in PE99, the strength of wave drag is an important modulator of the upwelling response. This is especially true if one takes wave-drag as an external forcing on the system.

However, our work, like PE99, highlights the potential role that tropospheric thermal forcing may have on stratospheric upwelling. In fact, the theoretical analysis shown in PE99 finds that in the tropics, "the existence of a thermally driven circulation and the breakdown of downward control go together" (if one accepts that what they define as viscosity is representative of some large-scale drag). However, their calculation of the linear response to tropospheric thermal forcing exhibited large (and unrealistic) vertical penetration of the tropospheric circulation into the stratosphere. This work shows that this is most likely a result of their assumptions of the strength of radiative relaxation ($\alpha_{\text{rad}} = 10\,\text{days}^{-1}$) and viscosity ($\hat{D} = 500\,\text{days}^{-1}$). Assuming $S = 150$ (used in this study), this is equivalent to $\xi \approx 3$. In this regime, our theory predicts extensive penetration of the tropospheric circulation into the stratosphere, as in Figure 5. While estimation of D in the real world is a difficult task and out of the scope of this study, even reasonably weak values of $\hat{D} = 180\ \text{days}^{-1}$ lead to tropospherically-forced stratospheric upwelling of comparable magnitude to that of the Brewer-Dobson circulation. Thus, as highlighted in PE99, even small amplitude contributions to the angular momentum budget in the tropics can have seemingly large consequences on the circulation.

Our work also stresses the importance of the strength of radiative relaxation in the stratosphere. As such, ozone in the tropical lower stratosphere and TTL may also play a critical role in modulating the degree to which the troposphere can directly modulate stratospheric upwelling (Fueglistaler et al. 2011). Thus, there is reason to further investigate the role tropospheric thermal forcing (and subsequent radiative relaxation) has on stratospheric upwelling. As shown in this study, the vertical penetration of the geopotential anomaly (and the rate at which the stratospheric circulation crosses angular momentum surfaces) is strongly a function of the wave drag. In the absence of wave-drag, the geopotential in the stratosphere becomes barotropic when forced by a tropopause anomaly, though by our estimates, this takes a fairly long time. If the wave-drag is a function of time, the vertical penetration of the tropospheric forcing (and thus, the effect on upwelling) would also vary in time. In this view, stratospheric wave-drag is, as countless studies have shown, a significant modulator of and necessary for the Brewer-Dobson circulation. However, wave drag alone may not suffice to explain certain features of the behavior of the lower stratosphere, the foremost of which is the inverse correlation between SST and lower stratospheric temperature anomalies, in both the zonal and meridional directions.

There are a few pieces of observational evidence that could be interpreted to be in favor of the proposed theory. Of course, as stated earlier, in the tropics, anomalies in boundary layer temperature are highly correlated with tropopause temperature anomalies, on both global and regional scales (Holloway and Neelin 2007). In addition, there is a strong observed anti-correlation of temperature trends in the troposphere and the lower stratosphere (Fu et al. 2006). These long-term trends are highly correlated on a grid-point by grid-point basis, suggesting that the zonal and meridional structure of tropospheric warming may be important to that of stratospheric cooling. In contrast, wave-drag, in its classical arguments, can only explain departures of temperature from the zonal-mean (Andrews et al. 1987).

Stratospheric adjustment to tropopause forcing can explain not only the observed connection between boundary layer temperature anomalies and lower stratospheric temperature anomalies, but also the high correlations between tropical SST and the upwelling strength of the shallow BDC branch, on all time scales (Lin et al. 2015; Abalos et al. 2021). Numerical modeling suggests that strengthening of the sub-tropical jets changes the upward propaga-

tion of waves (Garcia and Randel 2008; Calvo et al. 2010; Shepherd and McLandress 2011), ultimately strengthening the wave-driven stratospheric upwelling, although the exact specifics seem to vary from model to model (Calvo et al. 2010; Simpson et al. 2011). In the zonally symmetric coupled troposphere-stratosphere theory analyzed in this work, an equatorial SST anomaly is not only associated with strengthening of the sub-tropical jets (which no doubt could change the wave-forcing in the real-world), but also a strengthening of the tropopause geopotential and upwelling in the lower tropical stratosphere. In contrast to theories based on tropospheric warming's modulation of wave-driving, strengthening of the tropopause geopotential is a direct route through which tropospheric warming can modulate stratospheric upwelling.

In the existing literature, it is hard to find numerical modeling experiments that can clearly distinguish between the effects of wave driving and steady tropospheric thermal forcing of the stratosphere. This is important if we want to understand which process imposes a larger footprint on tropopause temperature. For instance, Jucker and Gerber (2017) used idealized GCM simulations to show that the inclusion of a tropical warm pool significantly changed the annual-mean temperature of the tropical tropopause (and more importantly, more so than mid-latitude land-sea contrast and orographic forcing). However, it is difficult to separate the influence of the geostrophic adjustment process from that of wave forcing on the annual-mean tropopause temperature, since the imposition of a warm pool should also intensify the tropopause anti-cyclone. Separately, Ortland and Alexander (2014) forced equatorial waves by prescribing time-varying latent heating anomalies in a primitive equation model, and found that stationary waves and weakly westward propagating waves are most responsible for driving residual-mean upwelling in the TTL. Still, tropospheric heating drives a geopotential anomaly at the tropopause, and the distinction between upwelling induced by stationary waves as compared to quasi-steady, zonally asymmetric tropopause geopotential anomalies is unclear. Regardless, both of the modeling results in Ortland and Alexander (2014) and Jucker and Gerber (2017) show that at least in numerical models, the seasonal cycle in upwelling in the tropical tropopause layer cannot be explained by varying thermal forcing in the tropical troposphere.

It is only fair for these conclusions to be discussed alongside the assumptions posited in this model. In this model, we assume that there is an instantaneous transition between tropospheric, quasi-equilibrium dynamics, and passive, dry stratospheric dynamics. In reality, the presence of the TTL could serve to dampen the upwards influence of tropospheric forcing. Indeed, the assumption of a moist adiabatic lapse rate all the way to the tropopause is one that is has weak observational evidence, which suggests that the magnitude of free tropospheric temperature anomalies, per degree of warming in the boundary layer, are approximately moist adiabatic up to around 200-hPa, after which temperature anomalies transition to being out of phase with lower tropospheric temperature anomalies (Holloway and Neelin 2007). While the proposed theory can roughly predict the magnitude of the tropopause temperature anomalies with respect to boundary layer warming, it does not include a transition layer. The presence of a transition layer could, in theory, dampen the vertical penetration of thermal forcing in the troposphere.

In addition, we have restricted ourselves to only steady tropopause geopotential anomalies. This makes the analysis mathematically tractable. Indeed, there are variations in tropical SST on time scales longer than a year, to which this assumption would apply. However, there is also seasonal cycle that, in theory, could induce a seasonally reversing stratospheric circulation that is driven through tropospheric thermal forcing. The observations do not support this behavior in the tropical atmosphere, and this is perhaps because the timescale of the steady tropopause forcing needs to be much longer than the radiative relaxation time scale in the stratosphere.

Finally, we also assume a fixed tropopause height that interfaces the two regimes, as in PE99. Indeed, one would expect tropospheric temperature to affect tropopause height (Held 1982; Lin et al. 2017). The relaxation of both of these assumptions will be the subject of future research, but requires a theory for how moist convection interacts with the transition layer. More research is necessary to understand the role of convection in modulating the behavior of the transition layer, since basic fundamental questions, such as (1) "why is there a tropopause transition layer?", and (2) "what non-dimensional parameters describe its transition width?", seem to be yet unanswered.

Acknowledgments. The author thanks Adam Sobel and Peter Hitchcock for comments and suggestions on earlier versions of this work. J. Lin also gratefully acknowledges the support of the National Science Foundation through the NSF-AGS Postdoctoral Fellowship, under award number AGS-PRF-2201441.

Data availability statement. The monthly-mean ERA5 data for sea-surface temperature is available at `https://cds.climate.copernicus.eu/cdsapp#!/dataset/reanalysis-era5-single-levels-monthly-means` via DOI: 10.24381/cds.f17050d7 Hersbach et al. (2019b). The monthly-averaged ERA5 data for temperature and geopotential are available at `https://cds.climate.copernicus.eu/cdsapp#!/dataset/reanalysis-era5-pressure-levels-monthly-means` via DOI: 10.24381/cds.6860a573 Hersbach et al. (2019a). All code to generate the data from the theoretical models are available at `https://github.com/linjonathan/steady_coupled_trop_strat`.

References

Abalos, M., and Coauthors, 2021: The Brewer-Dobson circulation in CMIP6. *Atmospheric Chemistry and Physics Discussions*, 1–27.

Andrews, D. G., J. R. Holton, and C. B. Leovy, 1987: *Middle atmosphere dynamics*. 40, Academic press.

Birner, T., and H. Bönisch, 2011: Residual circulation trajectories and transit times into the extratropical lowermost stratosphere. *Atmospheric Chemistry and Physics*, **11 (2)**, 817–827.

Boehm, M. T., and S. Lee, 2003: The implications of tropical Rossby waves for tropical tropopause cirrus formation and for the equatorial upwelling of the Brewer–Dobson circulation. *J. Atmos. Sci.*, **60 (2)**, 247–261.

Butchart, N., 2014: The Brewer-Dobson circulation. *Rev. Geophys.*, **52 (2)**, 157–184.

Calvo, N., R. Garcia, W. Randel, and D. Marsh, 2010: Dynamical mechanism for the increase in tropical upwelling in the lowermost tropical stratosphere during warm ENSO events. *J. Atmos. Sci.*, **67 (7)**, 2331–2340.

Dima, I. M., and J. M. Wallace, 2003: On the seasonality of the Hadley cell. *J. Atmos. Sci.*, **60 (12)**, 1522–1527.

Dobson, G. M. B., 1956: Origin and distribution of the polyatomic molecules in the atmosphere. *Proceedings of the Royal Society of London. Series A. Mathematical and Physical Sciences*, **236 (1205)**, 187–193.

Emanuel, K. A., 1987: An air-sea interaction model of intraseasonal oscillations in the tropics. *J. Atmos. Sci.*, **44 (16)**, 2324–2340.

Emanuel, K. A., 1995: On thermally direct circulations in moist atmospheres. *J. Atmos. Sci.*, **52 (9)**, 1529–1534.

Fu, Q., C. M. Johanson, J. M. Wallace, and T. Reichler, 2006: Enhanced mid-latitude tropospheric warming in satellite measurements. *Science*, **312 (5777)**, 1179–1179.

Fueglistaler, S., A. Dessler, T. Dunkerton, I. Folkins, Q. Fu, and P. W. Mote, 2009: Tropical tropopause layer. *Rev. Geophys.*, **47 (1)**.

Fueglistaler, S., P. Haynes, and P. Forster, 2011: The annual cycle in lower stratospheric temperatures revisited. *Atmospheric Chemistry and Physics*, **11 (8)**, 3701–3711.

Garcia, R. R., and W. J. Randel, 2008: Acceleration of the Brewer–Dobson circulation due to increases in greenhouse gases. *J. Atmos. Sci.*, **65 (8)**, 2731–2739.

Garny, H., M. Dameris, W. Randel, G. E. Bodeker, and R. Deckert, 2011: Dynamically forced increase of tropical upwelling in the lower stratosphere. *J. Atmos. Sci.*, **68 (6)**, 1214–1233.

Gerber, E. P., 2012: Stratospheric versus tropospheric control of the strength and structure of the Brewer–Dobson circulation. *J. Atmos. Sci.*, **69 (9)**, 2857–2877.

Haynes, P., M. McIntyre, T. Shepherd, C. Marks, and K. P. Shine, 1991: On the "downward control" of extratropical diabatic circulations by eddy-induced mean zonal forces. *J. Atmos. Sci.*, **48 (4)**, 651–678.

Haynes, P. H., and M. E. McIntyre, 1987: On the evolution of vorticity and potential vorticity in the presence of diabatic heating and frictional or other forces. *J. Atmos. Sci.*, **44 (5)**, 828–841.

Held, I. M., 1982: On the height of the tropopause and the static stability of the troposphere. *J. Atmos. Sci.*, **39 (2)**, 412–417.

Held, I. M., and A. Y. Hou, 1980: Nonlinear axially symmetric circulations in a nearly inviscid atmosphere. *J. Atmos. Sci.*, **37 (3)**, 515–533.

Hersbach, H., and Coauthors, 2019a: ERA5 monthly averaged data on pressure levels from 1979 to present. *Copernicus Climate Change Service (C3S) Climate Data Store (CDS)*.

Hersbach, H., and Coauthors, 2019b: ERA5 monthly averaged data on single levels from 1979 to present. *Copernicus Climate Change Service (C3S) Climate Data Store (CDS)*.

Hitchcock, P., T. G. Shepherd, and S. Yoden, 2010: On the approximation of local and linear radiative damping in the middle atmosphere. *J. Atmos. Sci.*, **67 (6)**, 2070–2085.

Holloway, C. E., and J. D. Neelin, 2007: The convective cold top and quasi equilibrium. *J. Atmos. Sci.*, **64 (5)**, 1467–1487.

Holton, J. R., P. H. Haynes, M. E. McIntyre, A. R. Douglass, R. B. Rood, and L. Pfister, 1995: Stratosphere-troposphere exchange. *Rev. Geophys.*, **33 (4)**, 403–439.

Jensen, E., and L. Pfister, 2004: Transport and freeze-drying in the tropical tropopause layer. *J. Geophys. Res. Atmos.*, **109 (D2)**.

Jucker, M., and E. Gerber, 2017: Untangling the annual cycle of the tropical tropopause layer with an idealized moist model. *J. Climate*, **30 (18)**, 7339–7358.

Kerr-Munslow, A., and W. Norton, 2006: Tropical wave driving of the annual cycle in tropical tropopause temperatures. part I: ECMWF analyses. *J. Atmos. Sci.*, **63 (5)**, 1410–1419.

Kim, J., W. J. Randel, T. Birner, and M. Abalos, 2016: Spectrum of wave forcing associated with the annual cycle of upwelling at the tropical tropopause. *J. Atmos. Sci.*, **73 (2)**, 855–868.

Lin, J., and K. Emanuel, 2022: On the effect of surface friction and upward radiation of energy on equatorial waves. *J. Atmos. Sci.*, **79 (3)**, 837–857.

Lin, P., Y. Ming, and V. Ramaswamy, 2015: Tropical climate change control of the lower stratospheric circulation. *Geophys. Res. Lett.*, **42 (3)**, 941–948.

Lin, P., D. Paynter, Y. Ming, and V. Ramaswamy, 2017: Changes of the tropical tropopause layer under global warming. *J. Climate*, **30 (4)**, 1245–1258.

Norton, W., 2006: Tropical wave driving of the annual cycle in tropical tropopause temperatures. part II: Model results. *J. Atmos. Sci.*, **63 (5)**, 1420–1431.

Orbe, C., and Coauthors, 2020: GISS Model E2. 2: A climate model optimized for the middle atmosphere—2. validation of large-scale transport and evaluation of climate response. *J. Geophys. Res. Atmos.*, **125 (24)**, e2020JD033 151.

Ortland, D. A., and M. J. Alexander, 2014: The residual-mean circulation in the tropical tropopause layer driven by tropical waves. *J. Atmos. Sci.*, **71 (4)**, 1305–1322.

Plumb, R. A., 2002: Stratospheric transport. *Journal of the Meteorological Society of Japan. Ser. II*, **80 (4B)**, 793–809.

Plumb, R. A., and J. Eluszkiewicz, 1999: The Brewer–Dobson circulation: Dynamics of the tropical upwelling. *J. Atmos. Sci.*, **56 (6)**, 868–890.

Randel, W. J., R. Garcia, and F. Wu, 2008: Dynamical balances and tropical stratospheric upwelling. *J. Atmos. Sci.*, **65 (11)**, 3584–3595.

Randel, W. J., R. R. Garcia, N. Calvo, and D. Marsh, 2009: ENSO influence on zonal mean temperature and ozone in the tropical lower stratosphere. *Geophys. Res. Lett.*, **36 (15)**.

Randel, W. J., F. Wu, H. Voemel, G. E. Nedoluha, and P. Forster, 2006: Decreases in stratospheric water vapor after 2001: Links to changes in the tropical tropopause and the Brewer-Dobson circulation. *J. Geophys. Res. Atmos.*, **111 (D12)**.

Ryu, J.-H., and S. Lee, 2010: Effect of tropical waves on the tropical tropopause transition layer upwelling. *J. Atmos. Sci.*, **67 (10)**, 3130–3148.

Seviour, W. J., N. Butchart, and S. C. Hardiman, 2012: The Brewer–Dobson circulation inferred from ERA-Interim. *Quart. J. Roy. Meteor. Soc.*, **138 (665)**, 878–888.

Shepherd, T. G., and C. McLandress, 2011: A robust mechanism for strengthening of the Brewer–Dobson circulation in response to climate change: Critical-layer control of subtropical wave breaking. *J. Atmos. Sci.*, **68 (4)**, 784–797.

Simpson, I. R., T. G. Shepherd, and M. Sigmond, 2011: Dynamics of the lower stratospheric circulation response to ENSO. *J. Atmos. Sci.*, **68 (11)**, 2537–2556.

Sobel, A. H., and C. S. Bretherton, 2000: Modeling tropical precipitation in a single column. *J. Climate*, **13 (24)**, 4378–4392.

Taguchi, M., 2009: Wave driving in the tropical lower stratosphere as simulated by waccm. part i: Annual cycle. *J. Atmos. Sci.*, **66 (7)**, 2029–2043.